Geology, published online on 5 February 2015 as doi:10.1130/G36336.1

The role of bubbles in generating fine ash during hydromagmatic eruptions

E.J. Liu[1]*, K.V. Cashman[1], A.C. Rust[1], and S.R. Gislason[2]
[1]Earth Sciences, University of Bristol, Wills Memorial Building, Bristol BS8 1RJ, UK
[2]Institute of Earth Sciences, University of Iceland, Sturlugata 7, 101 Reykjavík, Iceland

ABSTRACT

The abundant fine ash produced in the 2011 subglacial eruption of Grímsvötn, Iceland, highlights the fragmentation efficiency of mafic hydromagmatic eruptions, which is considerably higher than for comparable "dry" eruptions. Ash from the 2011 eruption can be divided into three morphological components—vesicular particles, shards, and dense fragments—distinguished by the size and abundance of constituent vesicles. We use the vesicle characteristics to define a new shape factor, the concavity index, which provides an unbiased way to classify individual ash particles as either bubbly (vesicular particles and shards) or dense. The relative proportion of bubbly and dense particles varies systematically with grain size, with the proportion of bubbly grains decreasing as the particle size approaches the modal bubble diameter. Measured bubble volume distributions are similar to those of rapidly quenched pyroclasts from Hawaiian fountains and suggest a comparable degassing history during magma ascent. Yet concordance between the size distributions of ash and of bubbles in the Grímsvötn samples stands in contrast to the size distributions in Hawaiian fountains, where pyroclasts are orders of magnitude larger than individual bubbles. We propose that the Grímsvötn ash formed by brittle disintegration of vesicular pyroclasts and that fragmentation efficiency was amplified by residual thermal stresses in glass quenched by glacial water. The strong control of resulting particle sizes and morphologies by the size and spatial distribution of bubbles demonstrates that the bubble population cannot be ignored when modeling hydromagmatic fragmentation.

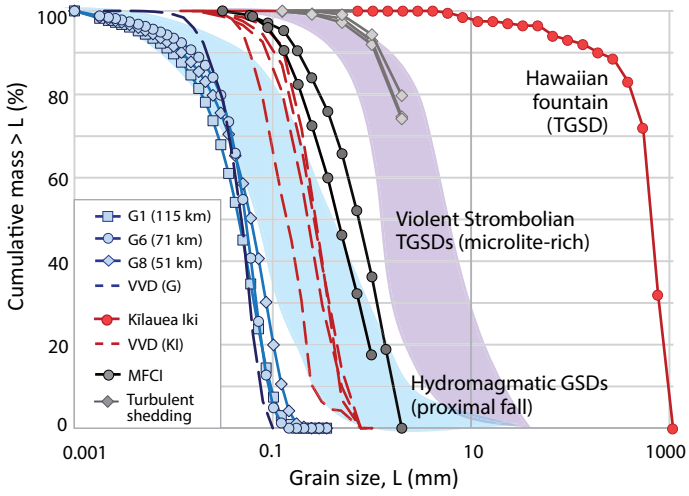

Figure 1. Grain size (GSD) and vesicle volume (VVD) distributions for Grímsvötn, Iceland (50–115 km from the 2011 vent; blue lines and symbols), and Kīlauea Iki, Hawai'i (total grain size distribution, TGSD; red lines and symbols). Representative GSDs for experimental products of molten fuel coolant interactions (MFCI) and "turbulent shedding" are shown for comparison. Blue and purple fields highlight typical GSDs for proximal hydromagmatic (<1 km from vent) and violent Strombolian (TGSDs) fall deposits, respectively. GSDs refer to size distributions at specific locations, whereas TGSDs incorporate many individual GSDs from different locations. All data and sources are presented in the Data Repository (Table DR3; see footnote 1).

INTRODUCTION

Recent eruptions in Iceland have highlighted the hazards of volcanic ash, in general, and of fine (suspended) ash in particular. In fact, the economic and societal disruption caused by the opening hydromagmatic phases of the 2010 Eyjafjallajökull and 2011 Grímsvötn eruptions derived in part from problems in determining appropriate ash grain size distributions (GSDs) as source terms for dispersion models. Source term uncertainties arise from the limited grain size data available for mafic hydromagmatic eruptions, which, in contrast to silicic systems, are profoundly different for "dry" and "wet" eruptions (Fig. 1). Moreover, medial to distal samples (50–115 km from vent) from the early phases of the 2011 Grímsvötn eruption are uniformly fine grained, even when considered in the context of published examples of mafic hydromagmatism (e.g., Murtagh and White, 2013). Explaining these data requires examination of fragmentation conditions promoted by magma-water interaction (MWI).

Fine fragmentation by MWI is commonly described by molten fuel coolant interaction (MFCI), where rapid heat transfer across silicate melt–water interfaces causes vapor explosion and brittle melt fragmentation (Zimanowski et al., 1997). Fragmentation may occur also by "turbulent shedding" (Mastin et al., 2004, 2009), where ash forms by disaggregation of glassy rinds formed on larger particles by contact with water. In turbulent shedding, fragmentation is aided by thermal contraction accompanying cooling. GSDs produced by both MFCI and turbulent shedding experiments are considerably coarser than for natural samples, however, even when the most proximal hydromagmatic fall deposits are considered (Fig.1).

We present a study of magma fragmentation during the 2011 Grímsvötn eruption, and generalize the results to MWI involving bubble-bearing mafic melts. With >60 known eruptions in the past 800 yr, Grímsvötn has been the most historically active, and compositionally uniform, volcanic system in Iceland (49–52 wt% SiO_2; Guðmundsson et al., 2012; Table DR1 in the GSA Data Repository[1]). Eruptions from the subglacial Grímsvötn central volcano are typically hydromagmatic, as erupting magma interacts with a subglacial caldera lake and the overlying glacier ice. The 21–28 May 2011 eruption was the largest in more than a century, producing 0.6–0.8 km^3 of pyroclastic material, mostly during the early (21–22 May) hydromagmatic activity (Hreinsdóttir et al., 2014). We examined the morphology and texture of hydromagmatic ash collected on 22 May 2011. Importantly, we analyze separately the componentry of ash particles in different size fractions and use both external morphology and internal texture to classify ash components. Together these data illustrate the critical role of bubbles on the GSD and, by inference, the fragmentation process.

METHODS

Ash samples were collected 50–115 km from the eruptive vent, either directly from the plume or from the ground shortly after deposition (Fig. DR1 in the Data Repository; Olsson et al., 2013). Samples were

*E-mail: emma.liu@bristol.ac.uk

[1]GSA Data Repository item 2015086, supplementary figures, Table DR1 (glass compositions), Table DR2 (image acquisition metadata), and Table DR3 (grain size distributions for Figure 1), is available online at www.geosociety.org/pubs/ft2015.htm, or on request from editing@geosociety.org or Documents Secretary, GSA, P.O. Box 9140, Boulder, CO 80301, USA.

sieved into four size fractions (3.5φ, 4φ, 5φ, and >5φ, corresponding to >91 µm, 63–91 µm, 32–63 µm, and <32 µm, respectively), mounted in epoxy and polished for scanning electron microscopy (SEM) in backscattered electron mode (BSE) at the University of Bristol (UK). The same size fractions were mounted on carbon stubs and gold coated for secondary electron (SE) microscopy. All high-resolution SEM images were obtained at a working distance of ~18.0 mm and either a 20 kV (SE) or 15kV (BSE) accelerating voltage. Particle shapes were quantified using numerical shape parameters (e.g., Dellino and La Volpe, 1996) measured in ImageJ software (imagej.nih.gov/ij/; data are available from the University of Bristol's data repository [DOI: 10.5523/bris.765l15d6gbsj1vty17u2a8ky2]. BSE images of particle cross-sections were deemed most suitable for shape analysis as they show both internal textures and external morphology, and highlight variations in particle contour more effectively than the projected area of three-dimensional (3-D) objects.

Bubble microtextures were quantified from vesicular ash particles and shards where at least 50% of the bubble wall was preserved (Fig. DR2). Bubble diameters were measured in 2-D using particles >91 µm; data were binned geometrically (Sahagian and Proussevitch, 1998) and converted to 2-D number densities (N_a) by normalizing to the total vesicle-free area of all particles (dense and vesicular) within the measured image. 3-D number densities (N_v) were determined by dividing N_a by the corresponding median diameter for each bubble size class (Mangan et al., 1993). Vesicle volume distributions (VVDs) were calculated by multiplying N_v for each size class by the volume of a sphere of equivalent diameter.

RESULTS

Grímsvötn ash contains only sparse microlites within a glassy (and bubbly) matrix. From SEM images in both 2-D (BSE) and 3-D (SE), we identified three main components: dense fragments, shards, and vesicular particles (Fig. 2). SE images show evidence of both fluidal and brittle deformation, even in the same particle. Brittle fracture surfaces preserve complex surface features (e.g., step fractures and river-line patterns; Fig. DR3), suggesting that fracturing occurred under mixed-mode regimes (Hull, 1999). Many surfaces are coated by dense adhering particles (<<10 µm) with fracture patterns similar to those of larger dense fragments, suggesting that a common generative process operated at a range of scales.

Dense fragments are poorly vesicular and angular with planar surfaces (Fig. 2B), and comprise both thin (commonly curved) platy grains and equant blocky grains. Shards and vesicular particles are angular and moderately to highly vesicular. Shards are characterized by highly concave outlines with smooth surfaces from large bounding vesicles. Internal vesicles are circular in cross-section with thin bubble walls (Fig. 2C). Vesicular particles contain numerous small (mostly spherical) vesicles separated by thicker bubble walls (Fig. 2D); shapes are equant with scalloped edges formed by bounding vesicles with diameters much smaller than that of the particle.

Morphological variations among the three components are determined by the shape and size of constituent vesicles, as manifested by variations in the surface roughness (concavity) of particle outlines: dense particles show little concavity, vesicular particles have small-scale concavities, and shards have particle-scale concavities. Concave indentations are best measured using shape parameters that compare size measures of 2-D particle outlines (e.g., area [A] and perimeter [P]) to those of the corresponding "convex hull" (ch; Fig. DR2), with solidity ($S = A/A_{ch}$) a measure of deficit area and convexity ($C = P_{ch}/P$) a measure of excess perimeter relative to the fully convex shape (where $S = C = 1$; Heilbronner and Barrett, 2013). To quantify differences in overall concavity, we combine these area- and perimeter-based shape parameters to define a composite parameter that we call the concavity index (CI):

$$\mathrm{CI} = \sqrt{(1-S)^2 + (1-C)^2}. \quad (1)$$

Dense fragments and bubbly shards represent the low-CI and high-CI end members respectively, while vesicular particles tend toward intermediate CI values (Fig. DR4). A comparison of CI and axial ratio (AR, ratio of minor to major axes of best fit ellipse) values for two calibrated (manually classified) ash size fractions (Fig. 2E) shows that CI = 0.4 effec-

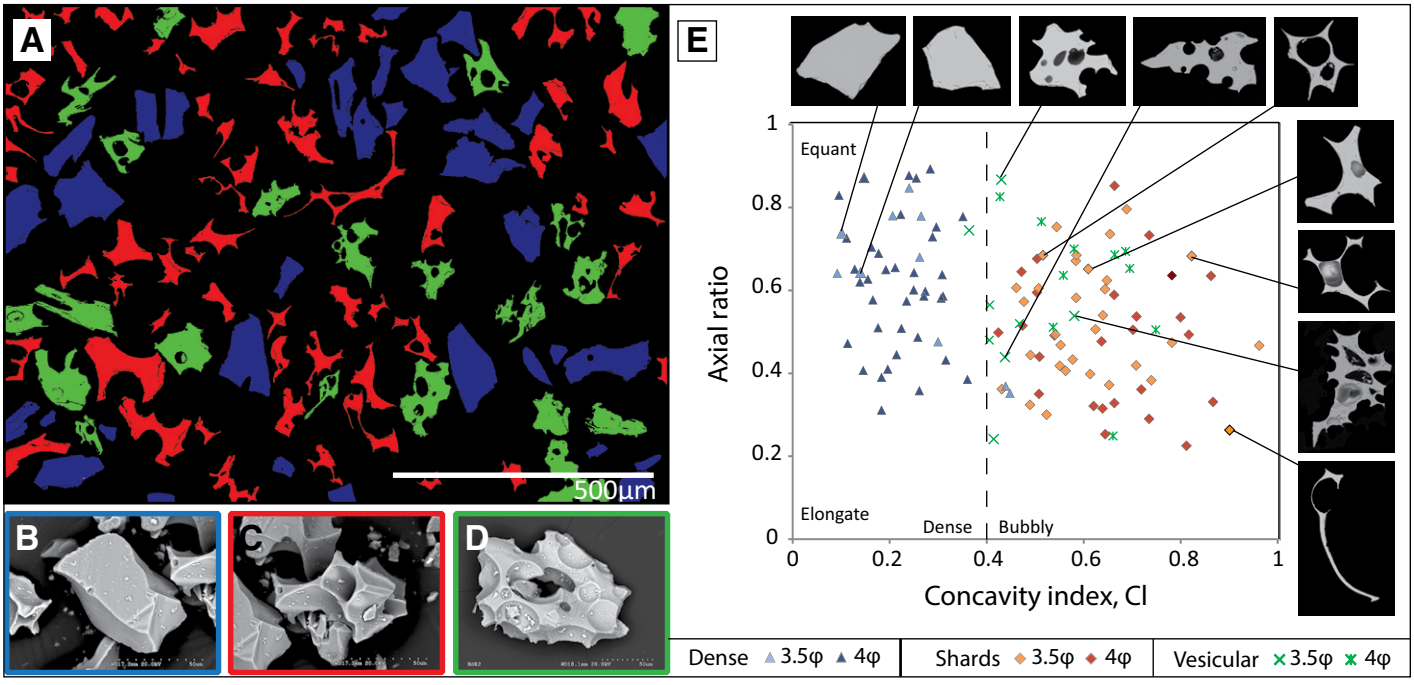

Figure 2. Ash characterization by shape analysis. A: Backscattered electron (BSE) image from <3.5φ (>91 µm) fraction of sample G6 with pseudo-color overlay highlighting dense fragments (blue), shards (red), and vesicular particles (green). B–D: Secondary electron (SE) images of the three components. E: Concavity index (CI) versus axial ratio, for components in B–D; dashed line at CI = 0.4 marks threshold between dense fragments and bubbly grains used for automated componentry.

tively separates the dense fragments (CI < 0.4) from shards and vesicular particles (CI > 0.4; sensitivity test shown in Fig. DR5). CI does not unambiguously discriminate between vesicular particles and shards; we therefore combine these into the single category of bubbly grains.

Applying a threshold of CI = 0.4 to BSE grid images for all samples and grain size classes (Fig. 3) shows that the proportion of bubbly relative to dense particles decreases systematically as the grain size decreases. Bubbly grains comprise 54%–63% of the >91 μm size fraction but only 19%–26% of the <32 μm size fraction. Manual classification of a subset of samples (dashed lines in Fig. 3) shows the same general trends but also highlights an increase in the proportion of bubbly grains with dispersal distance. This trend is particularly evident for the coarsest size fraction, where the proportion of bubbly grains increases with sampling distance from 72% at 50 km to 91% at 115 km.

Vesicle size distributions show a single mode between 15 and 25 μm (by number) or 50 and 60 μm (by volume; Fig. 1, blue dashed line "VVD"). Because the requirement for 50% bubble wall preservation prevents measurement of bubbles larger than the maximum grain dimension (~180 μm), we tested the distribution for truncation (Fig. DR6). Although there is no apparent truncation, concave curvature on even the largest shards is evidence of an unknown number of larger unmeasured vesicles (Fig. DR2). Bubble number densities range from 1.9 to 3.4 × 10^{13} m^{-3}.

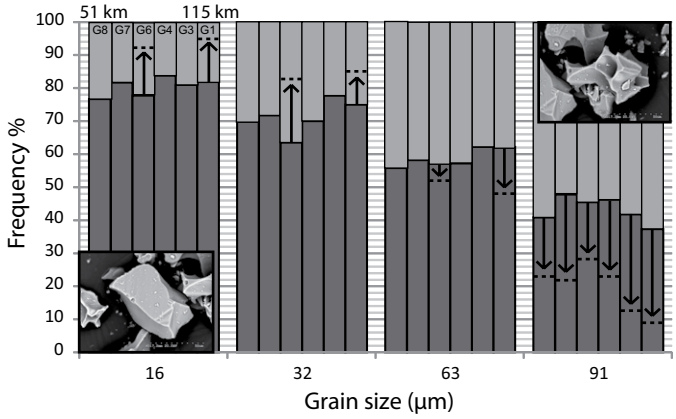

Figure 3. Variation in relative proportions of dense to bubbly (vesicular particles and shards) grains as function of size, shown by dark and light gray bars respectively. G8–G1 refer to samples 51–115 km from vent, respectively (Fig. DR1 [see footnote 1]). Shaded bars are derived from automated componentry (1159–3769 particles per size fraction; Table DR2) using the threshold concavity index of 0.4 (Fig. 2E). Dotted lines correspond to values from manual classification (>500 particles per size fraction).

DISCUSSION

Measurements of particle size, shape, and texture can be used to assess the efficiency and accuracy of different methods of ash classification, as well as the controls on magma fragmentation. Classification by both automated (CI) and manual methods shows clear increases in the proportion of dense particles with decreasing grain size, although the magnitude of the change is greater in the manual data (Fig. 3). This discrepancy results from two problems with automated componentry that do not affect visual particle classification: (1) particle clusters increase the apparent complexity of particle shape, and (2) small adhering particles increase apparent particle perimeters. Despite these caveats, CI effectively captures grain size–dependent trends in ash morphology (Fig. 2) and therefore provides a tool for rapid, reproducible, and objective ash characterization.

The key result of the shape analysis is the relationship between ash morphology and bubble microtexture. Specifically, differences in convexity and solidity (combined as CI) among ash components demonstrate that the size of bounding vesicles (if any) relative to the particle determines the grain morphology. Further evidence that bubble size controls morphology is provided by the variation in componentry as a function of grain size, whereby the proportion of dense fragments increases systematically as the particle size approaches the modal vesicle diameter. A comparison of the GSD and VVD shows that the means of the VVD and GSD are almost identical (Fig. 1), although the VVD is slightly narrower (smaller standard deviation). Together, these relationships suggest a key role for bubbles in the fragmentation process: the overall shape and size characteristics of Grímsvötn ash particles are a consequence of the size and spatial distribution of the pre-fragmentation bubble population, which in turn is controlled by conditions of bubble nucleation and growth during magma ascent.

The vesicle characteristics of the Grímsvötn ash—both VVDs and the dominance of isolated spherical vesicles—are similar to those of rapidly quenched pyroclasts from Hawaiian fountains (Porritt et al., 2012), although even small Pele's tears from Kīlauea record a slightly larger mean bubble size (Fig. 1, red dashed lines). Grímsvötn and Kīlauea differ, however, in the relation between VVDs and GSDs. Hawaiian eruptions produce clasts much larger than individual bubbles, whereas the Grímsvötn eruption produced ash with a mean size nearly identical to the mean bubble size. The latter relationship is also seen in silicic eruptions (Rust and Cashman, 2011), where bubble-bubble interaction controls fragmentation. We interpret the Grímsvötn data as evidence that fragmentation was controlled in large part by the bubble population, but by a different mechanism than for silicic eruptions. Grímsvötn ash particles are basaltic in composition (low viscosity), preserve evidence of both fluidal and brittle fragmentation, and have relatively thick bubble walls (indicating limited bubble expansion), all of which argue against fragmentation controlled by either strain rate (Dingwell and Webb, 1989) or vesicularity (Sparks, 1978). Instead, conditions for brittle fragmentation were established by rapid quenching of already actively vesiculating melt droplets by eruption through the subglacial lake.

Role of Bubbles in Fragmentation by Magma-Water Interaction

Although vesicular pyroclasts are common in hydromagmatic deposits (e.g., Mastin et al., 2004; Murtagh and White, 2013), the role of primary (magmatic) bubbles in hydromagmatic fragmentation has not been fully considered. Instead, extensive brittle fragmentation is commonly interpreted as evidence of MFCI. Notably, experimental products of MFCI are not only much coarser than typical hydromagmatic ash samples (Fig. 1), but also lack the bubbly ash components (vesicular clasts and shards) that dominate most Grímsvötn grain size classes. These differences lead us to consider alternative fragmentation mechanisms.

High thermal stresses can develop as melt is quenched, particularly when slower interior cooling causes contraction relative to the rapidly cooled exterior. Spontaneous (explosive) fragmentation of glass by thermal stresses can occur either during quenching or later, by release of stored residual stresses (Chandrasekar and Chaudhri, 1994). In fact, "thermal granulation" is probably the primary fragmentation mechanism in submarine/subglacial hyaloclastites (Kokelaar, 1986), although the low H_2O and S contents and prevalence of dense fragments in hyaloclastite breccias suggest significant degassing prior to fragmentation (Banik et al., 2014). How does thermal granulation operate in vesiculating magma?

Our data suggest that, critically, bubbles control the geometry of fracturing. During quenching, the presence of vesicles locally amplifies the stress within the surrounding groundmass; the overall brittle strength of a vesicular material is therefore influenced by the abundance, spatial distribution, and size of vesicles (Heap et al., 2014). Our componentry (Fig. 3) provides data on the minimum distance between adjacent vesicles, while measured VVDs provide complementary information on the size distribution of bubbles. Taken together, the small mean bubble size and the inferred low vesicularity of the quenched melt are consistent with interrupted vesiculation; remnants of fluidal surfaces further suggest that

quenching occurred following (or synchronous with) fluidal fragmentation of the melt. Evidence for subsequent brittle fracture is best explained by extensive thermal granulation of the glassy droplets.

The Grímsvötn data are probably not unique. Indeed, hydromagmatic deposits typically contain particles that span a wide range of vesicularity and clast morphology (e.g., Mastin et al., 2004; Murtagh and White, 2013), and exhibit evidence for brittle fragmentation (e.g., Büttner et al., 2002). Based on these observations, we suggest that the multi-stage (fluidal + brittle) fragmentation process hypothesized for the early phases of the 2011 Grímsvötn eruption applies to hydromagmatic activity more generally. Key is the evidence for pre-fragmentation vesiculation and the influence of those primary bubbles on subsequent fluidal fragmentation, water quenching, cooling-related contraction, and resulting secondary brittle fragmentation.

CONCLUSIONS

Volcanic ash from the 2011 subglacial eruption of Grímsvötn, Iceland, provides important insights into hydromagmatic fragmentation, particularly the mechanisms of fine ash generation. Ash components comprise a range of morphologies and textures that can be separated into dense fragments, vesicular particles, and shards (the latter two referred to as bubbly particles); the relative proportion of bubbly particles decreases as the grain size approaches the modal vesicle diameter (15–25 μm). Fragmentation by MWI during the hydromagmatic phase of the 2011 Grímsvötn eruption was much more extensive than is observed in typical "dry" mafic eruptions, and the concordance between the size distributions of ash and bubbles suggests a key role for bubbles in determining the size and shape of pyroclasts.

Preservation of fluidal clast surfaces and abundant bubbly particles indicates primary vesiculation prior to brittle fragmentation, and yet the presence of dense fragments and thick bubble walls in vesicular particles argues against a fragmentation mechanism driven solely by bubble expansion. Our results contrast with MFCI theory in that we explain fine fragmentation by magmatic vesiculation followed by rapid quenching and brittle breakage (amplified by residual thermal stresses in glass quenched during MWI), which does not necessarily require pre-mixing of magma and water. We speculate that secondary brittle fragmentation may be enhanced, however, by rapid steam expansion resulting from MWI.

Our work also underlines the importance of analyzing ash components from all available size classes. It is common to analyze only the 4φ (63–125 μm) size range (e.g., Dellino and La Volpe, 1996), which contains the "active" particles in MCFI experiments. We have shown, however, that Grímsvötn ash contains abundant particles >4φ (<63 μm) and that ash morphology changes with grain size. Together these data yield important insight into the pre-eruptive state of the magma. Furthermore, changes in component proportions within a single size class as a function of transport distance provide critical input to dispersion models regarding the influence of particle shape and density on ash transport.

ACKNOWLEDGMENTS

We acknowledge support from the AXA Research Fund to Cashman, a Royal Society University Research Fellowship to Rust, and a University of Bristol scholarship to Liu. We thank D. Swanson, L. Mastin, R. Cioni, and J.K. Russell for their highly constructive reviews.

REFERENCES CITED

Banik, T.J., Wallace, P.J., Höskuldsson, Á., Miller, C.F., Bacon, C.R., and Furbish, D.J., 2014, Magma–ice–sediment interactions and the origin of lava/hyaloclastite sequences in the Síða formation, South Iceland: Bulletin of Volcanology, v. 76, 785, doi:10.1007/s00445-013-0785-3.

Büttner, R., Dellino, P., La Volpe, L., Lorenz, V., and Zimanowski, B., 2002, Thermohydraulic explosions in phreatomagmatic eruptions as evidenced by the comparison between pyroclasts and products from Molten Fuel Coolant Interaction experiments: Journal of Geophysical Research, v. 107, 2277, doi:10.1029/2001JB000511.

Chandrasekar, S., and Chaudhri, M.M., 1994, The explosive disintegration of Prince Rupert's drops: Philosophical Magazine B, v. 70, p. 1195–1218, doi:10.1080/01418639408240284.

Dellino, P., and LaVolpe, L., 1996, Image processing analysis in reconstructing fragmentation and transportation mechanisms of pyroclastic deposits: The case of Monte Pilato-Rocche Rosse eruptions, Lipari (Aeolian islands, Italy): Journal of Volcanology and Geothermal Research, v. 71, p. 13–29, doi:10.1016/0377-0273(95)00062-3.

Dingwell, D.B., and Webb, S.L., 1989, Structural relaxation in silicate melts and non-Newtonian melt rheology in geologic processes: Physics and Chemistry of Minerals, v. 16, p. 508–516, doi:10.1007/BF00197020.

Guðmundsson, M.T., et al., 2012, The May 2011 eruption of Grímsvötn: EGU General Assembly Conference Abstracts, v. 14, p. 12119.

Heap, M.J., Xu, T., and Chen, C.F., 2014, The influence of porosity and vesicle size on the brittle strength of volcanic rocks and magma: Bulletin of Volcanology, v. 76, 856, doi:10.1007/s00445-014-0856-0.

Heilbronner, R., and Barrett, S., 2013, Image Analysis in Earth Sciences: Microstructures and Textures of Earth Materials: Berlin, Springer, 520 p.

Hreinsdóttir, S., et al., 2014, Volcanic plume height correlated with magma-pressure change at Grímsvötn Volcano, Iceland: Nature Geoscience, v. 7, p. 214–218, doi:10.1038/ngeo2044.

Hull, D., 1999, Fractography: Observing, Measuring and Interpreting Fracture Surface Topography: Cambridge, UK, Cambridge University Press, 386 p.

Kokelaar, P., 1986, Magma-water interactions in subaqueous and emergent basaltic volcanism: Bulletin of Volcanology, v. 48, p. 275–289, doi:10.1007/BF01081756.

Mangan, M.T., Cashman, K.V., and Newman, S., 1993, Vesiculation of basaltic magma during eruption: Geology, v. 21, p. 157–160, doi:10.1130/0091-7613(1993)021<0157:VOBMDE>2.3.CO;2.

Mastin, L.G., Christiansen, R.L., Thornber, C., Lowenstern, J., and Beeson, M., 2004, What makes hydromagmatic eruptions violent? Some insights from the Keanakako'i Ash, Kīlauea Volcano, Hawai'i: Journal of Volcanology and Geothermal Research, v. 137, p. 15–31, doi:10.1016/j.jvolgeores.2004.05.015.

Mastin, L.G., Spieler, O., and Downey, W.S., 2009, An experimental study of hydromagmatic fragmentation through energetic, non-explosive magma–water mixing: Journal of Volcanology and Geothermal Research, v. 180, p. 161–170, doi:10.1016/j.jvolgeores.2008.09.012.

Murtagh, R.M., and White, J.D.L., 2013, Pyroclast characteristics of a subaqueous to emergent Surtseyan eruption, Black Point volcano, California: Journal of Volcanology and Geothermal Research, v. 267, p. 75–91, doi:10.1016/j.jvolgeores.2013.08.015.

Olsson, J., Stipp, S.L.S., Dalby, K.N., and Gislason, S.R., 2013, Rapid release of metal salts and nutrients from the 2011 Grímsvötn, Iceland volcanic ash: Geochimica et Cosmochimica Acta, v. 123, p. 134–149, doi:10.1016/j.gca.2013.09.009.

Porritt, L.A., Russell, J.K., and Quane, S.L., 2012, Pele's tears and spheres: Examples from Kīlauea Iki: Earth and Planetary Science Letters, v. 333–334, p. 171–180, doi:10.1016/j.epsl.2012.03.031.

Rust, A.C., and Cashman, K.V., 2011, Permeability controls on expansion and size distributions of pyroclasts: Journal of Geophysical Research, v. 116, B11202, doi:10.1029/2011JB008494.

Sahagian, D.L., and Proussevitch, A.A., 1998, 3D particle size distributions from 2D observations: Stereology for natural applications: Journal of Volcanology and Geothermal Research, v. 84, p. 173–196, doi:10.1016/S0377-0273(98)00043-2.

Sparks, R.S.J., 1978, The dynamics of bubble formation and growth in magmas: A review and analysis: Journal of Volcanology and Geothermal Research, v. 3, p. 1–37, doi:10.1016/0377-0273(78)90002-1.

Zimanowski, B., Büttner, R., Lorenz, V., and Häfele, H.G., 1997, Fragmentation of basaltic melt in the course of explosive volcanism: Journal of Geophysical Research, v. 102, p. 803–814, doi:10.1029/96JB02935.

Manuscript received 7 October 2014
Revised manuscript received 19 December 2014
Manuscript accepted 7 January 2015

Printed in USA

Geology

The role of bubbles in generating fine ash during hydromagmatic eruptions

E.J. Liu, K.V. Cashman, A.C. Rust and S.R. Gislason

Geology published online 5 February 2015;
doi: 10.1130/G36336.1